

EVIDENT: Routing MLLM Adaptation through Entity-Grounded Visual Evidence for Cross-Domain Video Temporal Grounding

Geo Ahn*
Kyung Hee University
ahngeo11@khu.ac.kr

Jiwook Han*
Kyung Hee University
mrreraser@khu.ac.kr

Youngrae Kim*
University of Southern California
youngrae@usc.edu

Joonseok Lee
Seoul National University
joonseok@snu.ac.kr

Jinwoo Choi[†]
Kyung Hee University
jinwoochoi@khu.ac.kr

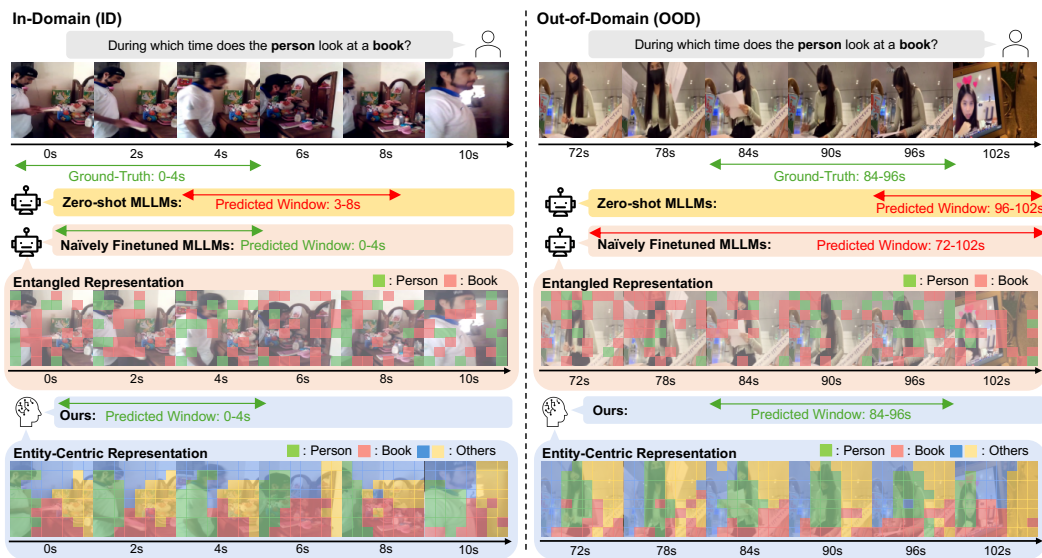


Figure 1: **Teaser.** In this work, we tackle the domain generalization problem of MLLM-based VTG. We observe that naively fine-tuned MLLMs learn entangled visual representations that rely on dataset-specific scene context rather than the actual visual content, indiscriminately responding to memorized patterns across frames in OOD videos. In contrast, our method learns an *entity-centric* visual representation that regularizes VTG fine-tuning to ground its predictions in the *visual evidence* of the video, yielding transferability to OOD domains. As a result, ours successfully captures both *person* and *book* consistently across frames and enables correct grounding regardless of the domain.

Abstract

Fine-tuning MLLMs for Video Temporal Grounding (VTG) often improves in-domain performance but degrades sharply under domain shift. In this work, we find that this failure is primarily driven not just by unseen query concepts, but by *visual domain shift*, which prevents the model from coupling its learned temporal

*Equal contribution.

[†]Corresponding author.

localization knowledge with its inherent entity-attention capability. To address this, we introduce EVIDENT, a parameter-efficient adaptation framework that anchors temporal grounding in the inherent entity-attention of pre-trained MLLMs by routing VTG adaptation through *explicit visual entity evidence*. EVIDENT consists of three components: (i) an Entity Bottleneck Adapter that transforms dense visual tokens into compact entity-level slots, (ii) an Entity-Binding Distillation loss that instills objectness priors into the semantically unstructured MLLM visual space, guiding each slot to bind to a coherent entity, and (iii) an Entity-to-eVidence gating mechanism that leverages the captured entities as evidence, steering the model to localize moments containing query-relevant entities. Together, these components enable VTG fine-tuning to rely on entity-grounded evidence rather than brittle dataset shortcuts. Experiments on cross-domain VTG benchmarks show that EVIDENT consistently improves out-of-domain robustness while preserving competitive in-domain performance with modest parameter overhead. These results suggest that entity-level grounding is an effective inductive bias for generalizable temporal localization.

1 Introduction

Video Temporal Grounding (VTG) requires localizing the temporal extent of an event described by a natural language query in an untrimmed video. While the task has been studied extensively with specialist temporal localization models such as DETR-based architectures [22, 35, 29, 42], Multimodal Large Language Models (MLLMs) have recently emerged as a compelling alternative [15, 40, 11, 44, 33, 51]. The appeal of MLLMs is not merely their scale. Through large-scale image-text and video-text pre-training, they acquire broad visual-language alignment that can associate language queries with relevant visual entities across diverse video domains.

However, VTG exposes a critical *adaptation paradox*. Before VTG-specific fine-tuning, pretrained MLLMs exhibit coarse but domain-agnostic *entity-attention capability*: given a query, they can often attend to semantically relevant visual content across different visual distributions (Figure 2 (a)). Yet this zero-shot attention is too coarse for VTG, which demands exact start and end timestamps, making task-specific fine-tuning necessary [15, 40, 44, 51, 33]. However, the extremely high cost of VTG annotations limits the scale and diversity of supervision, leaving source-domain fine-tuning vulnerable to shortcut learning—including temporal location bias [6, 38, 12], query text bias [6, 25, 17], and appearance bias [4, 39]. These shortcuts cause fine-tuning to rely on source-specific patterns rather than the underlying entity-attention, so the learned localization knowledge fails to inherit the MLLM’s domain-agnostic entity-attention. As a result, fine-tuning improves In-Domain (ID) localization but harms generalization under Out-of-Domain (OOD) scenarios where shortcuts no longer hold (Figure 1, Figure 2 (b)). We call this phenomenon *attention-localization decoupling* in OOD VTG.

In this work, we find that this decoupling is primarily driven by *visual domain shift*. We decompose the OOD gap into two factors: a *concept domain gap*, which captures whether the query involves subjects or actions unseen during source training, and a *visual domain gap*, which measures how visually distant the OOD videos are from the source distribution. Splitting OOD samples by query-concept overlap yields only a marginal performance difference (Figure 3 (a)). In contrast, splitting them by visual similarity to the source domain yields a substantially larger gap (Figure 3 (b)). These observations indicate that OOD degradation stems primarily from *visual domain shift*.

These findings point to a different *design principle* for cross-domain MLLM-based VTG: robust adaptation should anchor temporal localization in the *inherent entity-attention* of the pre-trained MLLM, rather than merely fitting dense visual tokens to source-domain scene context. To this end, we propose EVIDENT, a parameter-efficient framework for EVIDence-grounded ENTity-attentive adaptation for cross-domain VTG. Our goal is to learn transferable VTG knowledge by deriving temporal grounding predictions from *query-relevant visual entity evidence*. Realizing this principle requires three questions: (i) how to route adaptation through entities, (ii) what makes the entities meaningful, and (iii) how to leverage this entity information as evidence for temporal localization.

EVIDENT answers these questions with three key components. First, we propose an **Entity Bottleneck Adapter (EB Adapter)**, which routes intermediate MLLM dense visual tokens through a compact set of entity slots to obtain domain-invariant representations. Unlike prior works [46, 7, 24] that re-run instruction tuning to reshape MLLM representations into an entity-level form, our adapter design enables VTG learning grounded in entity-based visual representations at minimal cost. Second, we incorporate an **Entity-Binding Distillation (EB Distillation)** loss to encourage each slot to bind to

a *coherent* entity. We find that the pre-trained MLLM visual space alone has entangled representations and thus struggles to encode distinct entity information (Figure 1, Figure 11). In contrast, EVIDENT trained with our EB Distillation loss captures semantically coherent entities even under domain shift, as illustrated in Figure 1. Third, to leverage the entity information captured by EB Adapter with EB Distillation as *explicit visual evidence* guiding temporal localization predictions, we introduce an **Entity-to-evidence (E2V) gating** mechanism. Using the entity-attention of the pre-trained MLLM, we score each frame for the presence of query-relevant entities and modulate EB Adapter’s per-frame contribution accordingly. This injects an inductive bias that the target moment is where the query entities co-occur, enabling evidence-grounded localization under OOD shifts.

We evaluate EVIDENT under cross-domain VTG settings, training on a single source dataset and evaluating on different target datasets [10, 22, 13]. Across standard benchmarks, EVIDENT consistently improves OOD robustness while maintaining competitive ID performance with modest parameter and memory overhead. These results support our central claim: for robust MLLM-based VTG under visual domain shift, what is needed is evidence-grounded adaptation that fully leverages the pre-trained entity-attention, not direct fitting to source-domain context.

We summarize our contributions as follows:

- Through systematic analyses, we find that naïvely fine-tuning MLLMs causes *attention-localization decoupling*—the learned temporal localization fails to inherit the pre-trained entity-attention capability—and show that it is primarily driven by *visual domain shift*.
- We propose EVIDENT, a parameter-efficient framework for evidence-grounded entity-attentive adaptation in cross-domain VTG. Our entity bottleneck adapter with entity-binding distillation reshapes MLLM features into *entity-centric* representations without re-running instruction tuning, while the proposed entity-to-evidence gating leverages these entities as *explicit visual evidence* for temporal localization.
- We show that our evidence-grounded VTG adaptation yields consistent OOD robustness gains on diverse cross-domain VTG settings, while maintaining competitive in-domain performance with a modest number of parameters.

2 Related Work

Video Temporal Grounding Video Temporal Grounding (VTG) aims to localize the temporal segments in an untrimmed video that correspond to a natural language query. Recent works [15, 40] reformulate VTG as a generative task on MLLMs that produces temporal boundaries as text tokens via task-specific instruction tuning. Follow-up work refines this formulation through interleaved frame–timestamp representations [33, 28], causal event modeling [11], grounded tuning for long videos [51], chain-of-LoRA reasoning [30], and reinforcement learning with verifiable temporal rewards [43], all primarily relying on large-scale instruction tuning. While these efforts enhance the temporal capability of MLLMs, the fine-tuning step that is inevitably required for accurate localization remains an unexamined source of risk: these methods do not directly address the OOD generalization failure that this fine-tuning induces, which is the main issue we study.

Object-centric Learning Object-centric learning represents a scene as a composition of entity-level parts, yielding transferable representations under domain shifts. Slot attention [31] is a representative mechanism, where learnable slots iteratively compete to explain the input, and has been extended to real-world images [41] and videos [19, 45]. Recent work brings this idea into MLLMs: Slot-VLM [46] splits video tokens into object- and event-centric slots, Slot-MLLM [7] combines a Q-Former with slot attention for unified multimodal generation, and CORE [24] compresses visual tokens into a compact set of slots for efficient MLLM inference, using segmentation masks from an off-the-shelf model as an object-centric prior. However, all of these approaches require training the entire vision-language pipeline from scratch, whereas EVIDENT introduces a parameter-efficient EB Adapter attachable to pre-trained MLLMs, bringing entity-centric structure while preserving the pretrained vision-language alignment.

3 Problem Analysis

To understand why naïvely fine-tuned MLLMs suffer under domain shift, we conduct a series of empirical analyses. We fine-tune Qwen2.5-VL-7B [3] and InternVL3-2B [53] on Charades-STA

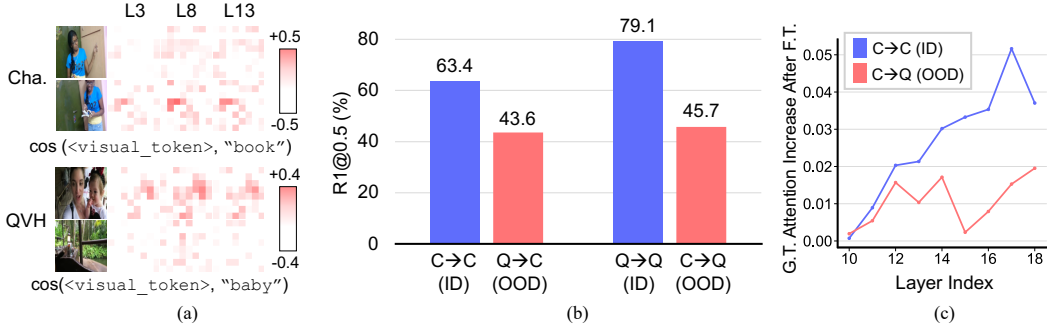


Figure 2: **Naïve fine-tuning breaks generalization.** (a) Cosine similarity between visual patches and object text tokens from Qwen2.5-VL-3B [3] on Charades-STA (Cha.) [10] and QVHighlights (QVH) [22]. Even zero-shot, the MLLM exhibits strong visual-text alignment regardless of video domain. (b) When fine-tuned on a specific domain, the model suffers severe OOD drops. (c) The model’s attention on GT-interval frames relative to all frames increases substantially on the source domain (ID) but only marginally on the unseen domain (OOD), indicating that the learned VTG capability fails to transfer to other domains.

(Cha.) [10] and evaluate on QVHighlights (QVH) [22]. See the supplementary material for the InternVL3 [53] results and more details.

3.1 OOD Failure Observations

Pre-trained MLLMs exhibit strong entity-attention capability. We first measure the visual-text alignment of the pre-trained Qwen2.5-VL-3B [3] by computing the cosine similarity between visual patches and object text tokens. As shown in Figure 2 (a), the pre-trained model exhibits strong visual-text alignment across visually distinct domains (Cha. [10] and QVH [22]), with high similarity between object text tokens (e.g., ‘book’) and the corresponding visual patches at the frame level. This indicates that the inherent *entity-attention* ability of pre-trained MLLMs to associate language queries with relevant visual content already transfers across diverse video distributions.

Naïve fine-tuning causes severe OOD performance degradation. While the pre-trained model shows transferable alignment, naïvely fine-tuning it on a single source dataset breaks this transferability (Figure 2 (b)). Fine-tuning on Cha. [10] produces a 19.8-point ID-OOD gap on QVH [22], and fine-tuning on QVH [22] produces a 33.4-point gap on Cha. [10]. The fine-tuned model overfits to source-domain patterns, failing to generalize to unseen domains.

Acquired grounding capability fails to transfer. To probe the source of this collapse, we measure how strongly the fine-tuned model’s visual-to-query cross-attention shifts toward ground-truth-interval frames, relative to the zero-shot baseline (Figure 2 (c)). We focus on layers 10–18, following prior findings that visual-language interaction in VideoLLMs primarily occurs at intermediate layers [18]. Fine-tuning shifts attention toward ground-truth segments substantially on the trained domain (ID) but only marginally on the unseen domain (OOD), revealing that the learned localization does not transfer across domains.

3.2 Domain Gap Diagnosis

We next ask: *what is the primary cause of this transfer failure?* We decompose the domain gap into two sources, a *concept domain gap* (whether OOD samples involve query concepts unseen during training) and a *visual domain gap* (how visually distant OOD samples are from the source distribution), and analyze which one dominates. We provide an additional analysis of the correlation between these two gaps in the supplementary material (Section B.3).

Concept gap does not explain OOD failure. We split the OOD test set (QVHighlights [22]) by query-concept overlap with ID (Charades-STA [10]), separating samples whose query concepts appear in the source dataset from those that do not. As shown in Figure 3 (a), the performance gap between the two splits is marginal (3.7 points), indicating that pre-trained MLLMs already cover a broad range of concepts and the concept gap is not the dominant factor in OOD failure.

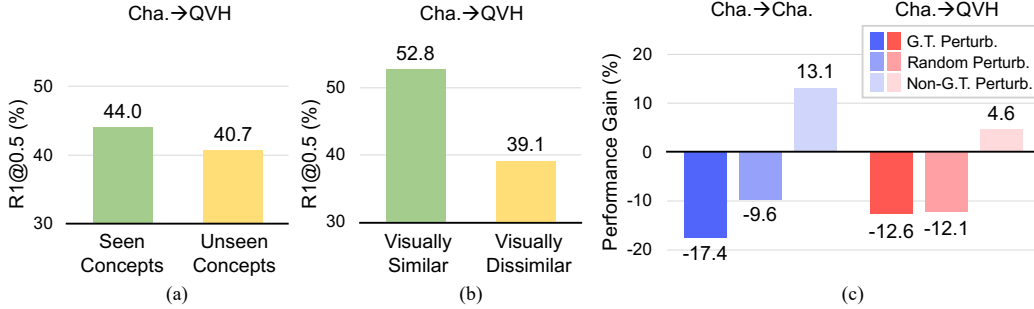


Figure 3: **Visual domain gap dominates.** We decompose the domain gap into *concept domain gap* and *visual domain gap*. (a) Splitting OOD samples by query-concept overlap with ID yields only a marginal gap. (b) Ranking OOD samples by visual similarity to ID, the top-20% most similar samples substantially outperform the bottom-20%, identifying the *visual domain gap* as the primary cause of degradation. (c) On ID, perturbing the G.T. interval causes a much larger drop than perturbing a random non-G.T. interval of the same length, while on OOD the two yield nearly identical drops.

Visual gap is the primary cause of OOD degradation. We instead split OOD samples by their visual feature similarity to the training set, where features are extracted from the vision encoder. As shown in Figure 3 (b), the most similar 20% of OOD samples achieve 52.8 R1@0.5, while the most dissimilar 20% drop to 39.1—a 13.7-point gap that scales with visual distance. This identifies the visual domain gap as the primary cause of OOD performance degradation.

The model ignores visual content under domain shift. To verify whether the model genuinely grounds its predictions in visual content, we inject Gaussian noise into either the ground-truth (G.T.) interval or a random non-G.T. interval of the same length and measure R1@0.7 drop. As shown in Figure 3 (c), on ID, G.T. perturbation causes a much larger drop than random (17.4% vs. 9.6%), while on OOD the two are nearly identical (12.6% vs. 12.1%)—the model no longer attends to the actual visual content under distribution shift. Conversely, injecting noise into the entire non-G.T. interval improves performance on both ID and OOD (+13.1% and +4.6%). It suggests that explicitly steering the model toward the visual content of the G.T. interval recouples its learned localization with the pre-trained entity-attention disrupted by visual domain shift, yielding gains even under OOD.

4 Method

We introduce **EVIDENT**, a parameter-efficient framework for cross-domain VTG that anchors temporal grounding in the inherent entity-attention of a pre-trained MLLM by injecting entity-centric visual representations at minimal cost. We describe the VTG task formulation (Section 4.1), EB Adapter (Section 4.2), EB Distillation (Section 4.3), E2V gating (Section 4.4), and the training objective (Section 4.5). Figure 4 (a) provides an overview.

4.1 VTG Task Formulation

Interleaved Timestamps. We follow the generative Video Temporal Grounding (VTG) paradigm, where an MLLM directly generates target timestamps as text tokens. Given T uniformly sampled video frames and a natural language query, we encode each frame into N visual tokens $\mathbf{f}_t \in \mathbb{R}^{N \times D}$ via a frozen vision encoder and a linear projector, where D is the hidden dimension of the LLM decoder, and tokenize its timestamp into a short text sequence τ_t . The input \mathbf{X} to the LLM decoder is constructed by interleaving each frame’s visual tokens with its timestamp tokens, followed by the query tokens \mathbf{q} :

$$\mathbf{X} = [\mathbf{f}_1, \tau_1, \mathbf{f}_2, \tau_2, \dots, \mathbf{f}_T, \tau_T, \mathbf{q}], \quad (1)$$

This interleaved layout has been shown to be effective for temporal grounding [33, 28, 52]. The model autoregressively decodes the target temporal window $[t_{\text{start}}, t_{\text{end}}]$.

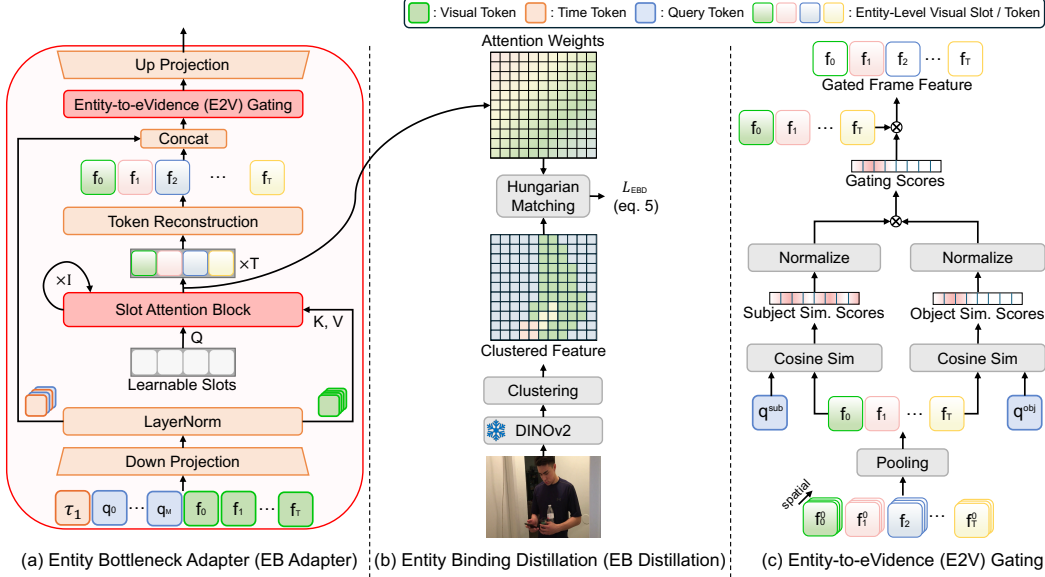


Figure 4: **Overview.** (a) **Entity Bottleneck Adapter (EB Adapter)**. A lightweight adapter in the early LLM decoder layers decomposes visual tokens into entity-level slots via slot attention. (b) **Entity Binding Distillation (EB Distillation)**. Entity cluster maps derived from DINOv2 [37] patch features are distilled into slot assignment maps via BCE loss, encouraging semantically coherent slot formation. (c) **Entity-to-eEvidence (E2V) Gating**. A per-frame gating score, reflecting the co-occurrence of query-relevant entities, modulates the adapter’s influence.

4.2 Entity Bottleneck Adapter

We propose Entity Bottleneck Adapter (EB Adapter), an adapter inserted into the MLLM decoder layers that reorganizes dense visual tokens into entity-based representations using a compact set of abstract slots. By leaving the original vision-language inference path and instruction alignment intact, EB Adapter *preserves the pre-trained entity-attention of the MLLM* while replacing only the domain-fragile dense visual representations with robust slot-based ones at minimal cost.

Down Projection. We first project the entire input sequence \mathbf{X} into a lower-dimensional bottleneck space: $\mathbf{X}_{\text{down}} = \mathbf{X}\mathbf{W}_{\text{down}} \in \mathbb{R}^{L \times d}$, where $\mathbf{W}_{\text{down}} \in \mathbb{R}^{D \times d}$ and $d \ll D$. From \mathbf{X}_{down} , we denote the visual portion as $\mathbf{X}_{\text{down}}^{\text{vis}} = [\mathbf{f}'_1, \dots, \mathbf{f}'_T] \in \mathbb{R}^{T \times N \times d}$ and the text portion as $\mathbf{X}_{\text{down}}^{\text{txt}} = [\mathbf{t}'_1, \dots, \mathbf{t}'_T, \mathbf{q}']$.

Slot Attention Block. A set of N_s learnable slot queries $\mathbf{S}^{(0)} \in \mathbb{R}^{N_s \times d}$ attend to the down-projected visual tokens $\mathbf{f}'_t \in \mathbb{R}^{N \times d}$ of each frame independently through I iterations. At iteration $i \in \{1, \dots, I\}$, we project the slots and the per-frame visual tokens into a common space: $\mathbf{Q}_t^{(i)} = \mathbf{S}_t^{(i-1)}\mathbf{W}_Q \in \mathbb{R}^{N_s \times d}$, $\mathbf{K}_t = \mathbf{f}'_t\mathbf{W}_K \in \mathbb{R}^{N \times d}$, and $\mathbf{V}_t = \mathbf{f}'_t\mathbf{W}_V \in \mathbb{R}^{N \times d}$, where \mathbf{W}_Q , \mathbf{W}_K , and \mathbf{W}_V are the projection matrices shared across frames. Next, the attention scores for frame t at iteration i are computed as:

$$\mathbf{M}_t^{(i)} = \mathbf{K}_t(\mathbf{Q}_t^{(i)})^\top / \sqrt{d} \in \mathbb{R}^{N \times N_s}. \quad (2)$$

We normalize $\mathbf{M}_t^{(i)}$ along the *slot axis* via softmax, fostering competitive assignment of visual tokens to slots within each frame:

$$\mathbf{A}_t^{(i)}(n, k) = \frac{\exp(\mathbf{M}_t^{(i)}(n, k))}{\sum_{j=1}^{N_s} \exp(\mathbf{M}_t^{(i)}(n, j))}. \quad (3)$$

We then normalize $\mathbf{A}_t^{(i)}$ along the token axis such that $\hat{\mathbf{A}}_t^{(i)}(\cdot, k)$ sums to one. The aggregated update is computed as a weighted mean $\mathbf{Z}_t^{(i)} = (\hat{\mathbf{A}}_t^{(i)})^\top \mathbf{V}_t \in \mathbb{R}^{N_s \times d}$, and the slots are then updated via a Gated Recurrent Unit (GRU) [8] based recurrence: $\mathbf{S}_t^{(i)} = \text{GRU}(\mathbf{S}_t^{(i-1)}, \mathbf{Z}_t^{(i)})$. This competition mechanism encourages each slot to specialize in a distinct semantic entity.

Token Reconstruction. Since the LLM decoder expects the original token sequence length, we reconstruct the visual tokens by reusing the slot attention’s assignment in a parameter-free manner. This design enforces that every reconstructed visual token is expressed only as a combination of slot features, thereby constraining the representations consumed by the LLM decoder to strictly adhere to *disentangled entity-level semantics*.

Given the final slot representations $\mathbf{S}_t^{(l)} \in \mathbb{R}^{N_s \times d}$ for frame t , we reconstruct token-level features as a weighted sum of slot features based on the slot attention’s assignment: $\tilde{\mathbf{f}}_t = \hat{\mathbf{A}}_t^{(l)} \mathbf{S}_t^{(l)} \in \mathbb{R}^{N \times d}$. We then concatenate the reconstructed visual portion $\tilde{\mathbf{X}}_{\text{down}}^{\text{vis}} = [\tilde{\mathbf{f}}_1, \dots, \tilde{\mathbf{f}}_T]$ with the unchanged text portion $\mathbf{X}_{\text{down}}^{\text{txt}}$ and project the result back to the original dimension via an up projection. The adapter output is added to the original input via a residual connection:

$$\mathbf{X}_{\text{out}} = \mathbf{X} + \text{concat}(\tilde{\mathbf{X}}_{\text{down}}^{\text{vis}}, \mathbf{X}_{\text{down}}^{\text{txt}}) \mathbf{W}_{\text{up}}, \quad (4)$$

where $\mathbf{W}_{\text{up}} \in \mathbb{R}^{d \times D}$ is initialized to zero, so the adapter acts as an identity mapping at the start of training. This ensures training stability while gradually steering the representations toward entity-level decomposition [14, 48].

Early-Layer Insertion. We attach the EB Adapter only to the early decoder layers. Recent findings [18] show that cross-frame interactions occur in these early layers, while deeper layers handle language integration and answer generation. By inserting the EB Adapter at this stage, each slot captures temporally coherent semantics across frames rather than frame-independent decompositions. The deeper layers, fine-tuned with LoRA [14, 48], then reason over these disentangled representations.

4.3 Entity Binding Distillation

While the EB Adapter encourages decomposition through its bottleneck structure, the bottleneck alone is insufficient: the entangled visual space of the naïve MLLM lacks the entity-level structure for slots to bind to. As a result, slots fail to specialize and produce near-uniform attention weights over visual tokens, as shown in Figure 11 (see Section D.1). To address this, we employ an Entity Binding Distillation (EB Distillation) loss. Inspired by prior works on object-centric learning [41, 1], our loss distills the objectness prior from a self-supervised vision model to encourage semantically coherent slot formation, as illustrated in Figure 4 (b).

Entity-level Matching. We extract DINOv2 [37] patch features from T frames, apply 2×2 average pooling to match the MLLM’s spatial resolution, and ℓ_2 -normalize along the feature dimension. We then perform K -means clustering ($K = N_s$) on each frame independently, yielding a binary cluster map $\mathbf{C} \in \{0, 1\}^{T \times K \times N}$, where $\mathbf{C}_{t,k,n} = 1$ indicates that patch n in frame t belongs to cluster k . Since slot and cluster indices are arbitrary, we perform per-frame Hungarian matching [20] between the normalized slot attention maps $\hat{\mathbf{A}} \in [0, 1]^{T \times K \times N}$ and \mathbf{C} , using patch-averaged BCE as the cost, to obtain an optimal one-to-one matching $\pi^{(t)} : \{1, \dots, K\} \rightarrow \{1, \dots, K\}$.

Loss. Given the matching, we define the alignment loss as the BCE between matched slot–cluster pairs, averaged over all frames, slots, and patches:

$$L_{\text{EBD}} = -\frac{1}{TKN} \sum_{t=1}^T \sum_{k=1}^K \sum_{n=1}^N \left[\mathbf{C}_{\pi^{(t)}(k),n}^{(t)} \log \hat{\mathbf{A}}_{k,n}^{(t)} + \left(1 - \mathbf{C}_{\pi^{(t)}(k),n}^{(t)}\right) \log \left(1 - \hat{\mathbf{A}}_{k,n}^{(t)}\right) \right]. \quad (5)$$

4.4 Entity to Evidence Gating

We introduce Entity-to-evidence (E2V gating) mechanism to leverage the entities captured by EB Adapter as explicit evidence for temporal grounding, injecting a VTG inductive bias that *temporal segments where query-relevant entities co-occur are more likely to be the target moment*. Specifically, we use the MLLM’s pretrained entity-attention to score per-frame entity presence and modulate EB Adapter’s output accordingly, as shown in Figure 4 (c).

Entity Extraction from Query. For each natural language query, we extract the subject and object concept words as query-relevant entities. We perform this offline using a pre-trained LLM (Qwen3-4B [47]) as a preprocessing step. We denote the extracted indices in the query token sequence as i_{sub} and i_{obj} . See the supplementary material for more details. Using these indices, we select the corresponding query tokens $\mathbf{q}'_{\text{sub}}, \mathbf{q}'_{\text{obj}} \in \mathbb{R}^d$ from the down-projected text portion $\mathbf{X}_{\text{down}}^{\text{txt}}$.

Frame-level Co-occurrence Score. We compute the cosine similarity between each frame’s averaged visual token and the subject/object query tokens: $s_t^{\text{sub}} = \cos(\bar{\mathbf{f}}_t, \mathbf{q}'_{\text{sub}})$, $s_t^{\text{obj}} = \cos(\bar{\mathbf{f}}_t, \mathbf{q}'_{\text{obj}})$, where $\bar{\mathbf{f}}_t \in \mathbb{R}^d$ is a per-frame visual representation obtained by averaging the N reconstructed visual tokens $\tilde{\mathbf{X}}_{\text{down}}^{\text{vis}}$. We then apply min-max normalization, yielding \hat{s}_t^{sub} and \hat{s}_t^{obj} . The final gating score for frame t is the product of the two normalized scores:

$$g_t = \hat{s}_t^{\text{sub}} \cdot \hat{s}_t^{\text{obj}} \in [0, 1]. \quad (6)$$

This product captures the co-occurrence of the subject and object: g_t is high only when both entities are present in frame t .

Gated Reconstruction. We modulate the reconstructed visual tokens by broadcasting the per-frame gating scores $\mathbf{g} = [g_1, \dots, g_T]$ across the N tokens within each frame, and replace the up projection step in the EB Adapter accordingly: $\mathbf{X}_{\text{out}} = \mathbf{X} + \text{concat}(\tilde{\mathbf{X}}_{\text{down}}^{\text{vis}} \odot \mathbf{g}, \mathbf{X}_{\text{down}}^{\text{txt}}) \mathbf{W}_{\text{up}}$, where \odot denotes element-wise multiplication with broadcasting along the token and feature dimensions. As a result, the EB Adapter’s contribution is concentrated on frames where query-relevant entities co-occur.

4.5 Training Objective

The framework is trained end-to-end with the vision encoder frozen. The EB Adapter and LoRA [14] parameters are updated jointly. We train EVIDENT with the combined objective $L_{\text{total}} = L_{\text{CE}} + \lambda L_{\text{EBD}}$, where λ controls the strength of the objectness prior.

5 Experiments

5.1 Experimental Setup

Training & Evaluation. We build on Qwen2.5-VL-Instruct [3] (7B) as the backbone MLLM and fine-tune it on two source datasets, Charades-STA (Cha.) [10] and QVHighlights (QVH) [22]. We evaluate the models on three target datasets: Cha., QVH, and DiDeMo [13]. Thanks to the parameter-efficient design of EVIDENT, only the EB Adapter and LoRA modules are trainable, amounting to approximately 201M parameters (2.36% of the 7B backbone). We denote each setting by its source-target pair (e.g., Cha.→QVH), reporting In-Domain (ID) performance when source equals target and Out-of-Domain (OOD) performance otherwise. All results are reported using the standard moment retrieval metrics R1@0.3, R1@0.5, R1@0.7, and mIoU.

Baselines. We compare EVIDENT against three categories of methods. (1) Large-scale instruction-tuned MLLMs for temporal grounding, evaluated in a zero-shot manner without any task-specific fine-tuning: HawkEye [44], TimeSuite [51], UniTime [28], and VideoMind [30]. (2) DETR-based specialists trained on a single source dataset: EaTR [16] and CG-DETR [34]. (3) MLLM-based methods fine-tuned on a single source dataset: Chrono [33] with a BLIP-2 [26] backbone, and Qwen2.5-VL [3] baseline fine-tuned with LoRA [14] under the same training setup as ours.

5.2 Results

Cross-domain VTG performance. Table 1 summarizes the results. EVIDENT consistently improves OOD performance across all source-target configurations while maintaining competitive ID performance. Among MLLM-based methods, we observe two failure modes that support our motivation presented in Section 1. First, zero-shot MLLMs, even those that are large-scale instruction-tuned, remain substantially below fine-tuned methods in the ID setting, confirming that task-specific adaptation is necessary for precise temporal localization. Second, naïve source-domain fine-tuning suffers severely under domain shift: although Qwen2.5-VL [3] reaches strong ID performance, its OOD R1@0.5 drops by over 23.9 points on Cha.→QVH and over 19.6 points on QVH→Cha. EVIDENT bridges these two regimes, delivering consistent OOD gains over the Qwen2.5-VL baseline (e.g., +5.5 R1@0.5 and +7.2 R1@0.7 on Cha.→QVH). These results demonstrate that entity-grounded visual evidence provides a robust pathway to fully leverage the entity-attention capabilities of pretrained MLLMs under domain shift.

What Do Slots Learn? In Figure 5, we visualize the slot attention maps of EVIDENT, fine-tuned on Cha. [10]. Across both ID (Cha.) and OOD (QVH, DiDeMo) samples, the slots decompose scenes into semantically coherent regions such as people, objects, and backgrounds. Importantly, this

Table 1: **Performance comparison on cross-domain video temporal grounding benchmarks.** We evaluate EVIDENT on Charades-STA [10], QVHighlights [22], and DiDeMo [13], reporting both In-Domain (ID) (source=target) and Out-of-Distribution (OOD) (source≠target) settings. † denotes our implemented baseline fine-tuned with LoRA [14]. Our results are highlighted; **bold** marks the best under each source→target setting. Zero-shot models are reported for reference, with cells left blank (-) for target datasets seen during their training.

Source dataset	Method	LLM size	Target dataset											
			Charades-STA				QVHighlights				DiDeMo			
			R1@0.3	R1@0.5	R1@0.7	mIoU	R1@0.3	R1@0.5	R1@0.7	mIoU	R1@0.3	R1@0.5	R1@0.7	mIoU
Zero-Shot	HawkEye [44]	7B	50.6	31.4	14.5	33.7	42.1	20.8	6.6	28.7	37.8	18.4	7.8	24.7
	TimeSuite [51]	7B	69.9	48.7	24.0	-	-	12.3	9.2	21.3	-	-	-	-
	UniTime [28]	7B	-	59.1	31.9	52.2	-	41.0	31.5	43.7	-	-	-	-
	VideoMind [30]	7B	73.5	59.1	31.2	50.2	-	-	-	-	-	-	-	-
Charades-STA	EaTR [16]	-	67.7	55.2	33.1	47.7	31.7	17.0	6.4	21.5	32.7	20.1	7.8	21.2
	CG-DETR [34]	-	69.7	57.6	35.1	49.5	37.4	22.8	10.5	25.2	30.3	21.8	11.0	20.7
	Chrono-BLIP [33]	4B	79.1	68.9	48.7	58.6	67.2	44.5	23.7	44.3	56.0	43.2	23.1	37.7
	Qwen2.5-VL† [3]	7B	80.3	67.7	43.9	58.1	75.2	54.3	29.7	51.2	68.2	53.8	30.3	47.4
	EVIDENT	7B	80.3	69.1	49.2	59.9	77.5	59.8	36.9	55.2	69.2	55.4	32.3	48.5
QVHighlights	EaTR [16]	-	40.8	27.2	13.0	28.0	70.3	59.6	40.3	53.1	36.0	17.8	6.5	24.1
	CG-DETR [34]	-	42.8	25.5	12.2	28.5	77.5	65.6	52.1	61.3	36.6	21.2	8.9	24.6
	Chrono-BLIP [33]	4B	63.3	39.3	20.4	42.7	86.1	76.6	62.7	70.7	43.0	24.4	11.8	33.7
	Qwen2.5-VL† [3]	7B	71.1	48.1	26.2	47.3	86.9	78.2	64.8	72.0	59.4	34.1	16.9	38.2
	EVIDENT	7B	73.3	50.2	28.0	49.0	89.5	82.2	69.1	75.3	62.4	36.0	17.4	40.6

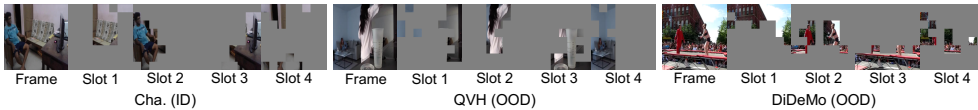


Figure 5: **EB Adapter attention visualization.** We visualize the attention map of EB Adapter (fine-tuned on Cha. [10]) on samples from Cha. (ID), QVH [22] (OOD), and DiDeMo [13] (OOD) by masking each frame with its highest-attending slot.

decomposition generalizes to unseen domains without any domain-specific supervision, confirming that EVIDENT learns *transferable entity-level representations* rather than source-biased patterns.

5.3 Ablation Study

Effects of EVIDENT components. We investigate the effect of each component of EVIDENT in Table 2 (a). Comparing the results with and without EB Distillation, we observe that applying the EB Adapter alone to the semantically unstructured MLLM visual space—as discussed in Section 4.3—fails to yield effective entity-centric representations. Only when our EB Distillation strategy is incorporated does the model learn transferable entity-level visual representations, leading to a gain in R1@0.5 by 3.9 points under the OOD setting. On top of this, the VTG-oriented inductive bias injected by E2V gating provides an additional 1.0-point improvement in OOD R1@0.5, confirming that the two components are complementary.

Effects of adapter design. In Table 2 (b), we show that attaching the learnable module to the MLLM decoder in an adapter style is the most effective placement for entity-level restructuring while preserving the pre-trained entity-attention. Compared to a variant that inserts a slot attention block between the vision encoder and the LLM decoder—which suffers a catastrophic performance collapse—our adapter-style design avoids disrupting the MLLM’s pre-trained alignment and still enables effective entity-level decomposition.

Effects of entity-level decomposition. In Table 2 (c), an adapter with standard self-attention improves ID R1@0.7 over LoRA [14] but suffers a severe OOD drop (-11.9 R1@0.5), indicating overfitting. In contrast, our EB Adapter maintains the ID gain and improves OOD by +5.5 R1@0.5, demonstrating that entity-level decomposition learns domain-invariant visual representations.

Effects of query-dependent E2V gating. In Table 2 (d), we compare two strategies for selecting the entities used to compute the gating score in E2V gating: extracting per-sample subject/object words from each query (query-dependent) versus using the fixed generic words, e.g., ‘person’ and ‘object’,

Table 2: **Ablation study.** To validate the effect of each component in EVIDENT, we show the results on the Cha.→QVH setting. We report R1@0.5 and R1@0.7 scores on both ID and OOD settings. The best numbers are **highlighted**.

(a) Effects of EVIDENT components.						(b) Effects of adapter design.					
EB Adapter	EB Distillation	E2V gating	Cha. (ID)		QVH (OOD)		Slot Attention Placement	Cha. (ID)		QVH (OOD)	
			R1@0.5	R1@0.7	R1@0.5	R1@0.7		R1@0.5	R1@0.7	R1@0.5	R1@0.7
			67.7	43.9	54.3	29.7					
✓			68.1	49.5	54.9	33.1	After vision encoder	34.6	18.8	19.5	12.7
✓	✓		69.1	50.4	58.8	36.7	Adapter-style (ours)	69.1	49.2	59.8	36.9
		✓	69.1	49.2	59.8	36.9					

(c) Effects of entity-level decomposition.						(d) Effects of query-dependent E2V gating.			
Bottleneck Design	Cha. (ID)		QVH (OOD)		Entity Source	Cha. (ID)		QVH (OOD)	
	R1@0.5	R1@0.7	R1@0.5	R1@0.7		R1@0.5	R1@0.7	R1@0.5	R1@0.7
LoRA [14]	67.7	43.9	54.3	29.7	Query-agnostic	69.3	49.4	58.4	36.0
Adapter w/ self-attn.	68.8	49.5	42.4	21.0	Query-dependent	69.1	49.2	59.8	36.9
EB Adapter	69.1	49.2	59.8	36.9					

for all samples (query-agnostic). The query-dependent variant yields a gain in OOD R1@0.5 by 1.4 points, demonstrating that our gating actively exploits the MLLM’s inherent entity-attention.

6 Conclusions

We presented **EVIDENT**, a parameter-efficient framework for cross-domain Video Temporal Grounding that anchors temporal localization in the inherent entity-attention of pre-trained MLLMs. Our analysis identifies *attention-localization decoupling* as a key failure in OOD VTG, which is primarily driven by visual domain shift rather than unseen query concepts. EVIDENT addresses this through three coupled components: an EB Adapter for routing visual tokens into entity-level slots, an EB Distillation loss for coherent slot bindings, and an E2V gating mechanism for entity-attention-based evidence grounding. Experiments on cross-domain VTG benchmarks show that EVIDENT consistently improves OOD robustness while maintaining competitive ID performance. Our results highlight that evidence-grounded entity-attentive adaptation, rather than direct fitting to source-domain context, is the key to robust cross-domain VTG.

References

- [1] Adil Kaan Akan and Yücel Yemez. Slot-guided adaptation of pre-trained diffusion models for object-centric learning and compositional generation. In *ICLR*, 2025. 7
- [2] Kyungho Bae, Geo Ahn, Younrae Kim, and Jinwoo Choi. DEVIAS: Learning disentangled video representations of action and scene. In *ECCV*, 2024. 13
- [3] Shuai Bai, Keqin Chen, Xuejing Liu, Jialin Wang, Wenbin Ge, Sibao Song, Kai Dang, Peng Wang, Shijie Wang, Jun Tang, Humen Zhong, Yuanzhi Zhu, Mingkun Yang, Zhaohai Li, Jianqiang Wan, Pengfei Wang, Wei Ding, Zheren Fu, Yiheng Xu, Jiabo Ye, Xi Zhang, Tianbao Xie, Zesen Cheng, Hang Zhang, Zhibo Yang, Haiyang Xu, and Junyang Lin. Qwen2.5-vl technical report. *arXiv preprint arXiv:2502.13923*, 2025. 3, 4, 8, 9, 14, 15, 16, 18
- [4] Peijun Bao and Yadong Mu. Learning sample importance for cross-scenario video temporal grounding. In *ICMR*, 2022. 2
- [5] Nicolas Carion, Francisco Massa, Gabriel Synnaeve, Nicolas Usunier, Alexander Kirillov, and Sergey Zagoruyko. End-to-end object detection with transformers. In *ECCV*, 2020. 13
- [6] Jinyeong Chae, Donghwa Kim, Kwansoek Kim, Doyeon Lee, Sangho Lee, Seongsu Ha, Jonghwan Mun, Wooyoung Kang, Byungseok Roh, and Joonseok Lee. Towards a complete benchmark on video moment localization. In *AISTATS*, 2024. 2, 13
- [7] Donghwan Chi, Hyomin Kim, Yoonjin Oh, Yongjin Kim, Donghoon Lee, Daejin Jo, Jongmin Kim, Junyeob Baek, Sungjin Ahn, and Sungwoong Kim. Slot-MLLM: Object-centric visual tokenization for multimodal llm. *arXiv preprint arXiv:2505.17726*, 2025. 2, 3
- [8] Kyunghyun Cho, Bart van Merriënboer, Caglar Gulcehre, Dzmitry Bahdanau, Fethi Bougares, Holger Schwenk, and Yoshua Bengio. Learning phrase representations using RNN encoder–decoder for statistical machine translation. In *EMNLP*, 2014. 6
- [9] Jinwoo Choi, Chen Gao, Joseph CE Messou, and Jia-Bin Huang. Why can’t i dance in the mall? learning to mitigate scene bias in action recognition. In *NeurIPS*, 2019. 13

- [10] Jiyang Gao, Chen Sun, Zhenheng Yang, and Ram Nevatia. Tall: Temporal activity localization via language query. In *ICCV*, 2017. 3, 4, 8, 9, 13, 14, 15, 16, 17, 18, 20, 21
- [11] Yongxin Guo, Jingyu Liu, Mingda Li, Xiaoying Tang, Qingbin Liu, and Xi Chen. TRACE: Temporal grounding video llm via causal event modeling. *arXiv preprint arXiv:2410.05643*, 2024. 2, 3
- [12] Jiachang Hao, Haifeng Sun, Pengfei Ren, Jingyu Wang, Qi Qi, and Jianxin Liao. Can shuffling video benefit temporal bias problem: A novel training framework for temporal grounding. In *ECCV*, 2022. 2, 13
- [13] Lisa Anne Hendricks, Oliver Wang, Eli Shechtman, Josef Sivic, Trevor Darrell, and Bryan Russell. Localizing moments in video with natural language. In *ICCV*, 2017. 3, 8, 9, 17, 18, 20, 21
- [14] Edward J Hu, Yelong Shen, Phillip Wallis, Zeyuan Allen-Zhu, Yuanzhi Li, Shean Wang, Lu Wang, and Weizhu Chen. Lora: Low-rank adaptation of large language models. In *ICLR*, 2022. 7, 8, 9, 10, 18, 19
- [15] Bin Huang, Xin Wang, Hong Chen, Zihan Song, and Wenwu Zhu. Vtimellm: Empower llm to grasp video moments. In *CVPR*, 2024. 2, 3
- [16] Jinhyun Jang, Jungin Park, Jin Kim, Hyeongjun Kwon, and Kwanghoon Sohn. Knowing where to focus: Event-aware transformer for video grounding. In *ICCV*, 2023. 8, 9, 13
- [17] Hao Jiang, Yang Yizhang, and Yadong Mu. Transferable video moment localization by moment-guided query prompting. In *AAAI*, 2024. 2
- [18] Minji Kim, Taekyung Kim, and Bohyung Han. Map the flow: Revealing hidden pathways of information in videollms. In *ICLR*, 2026. 4, 7, 19
- [19] Thomas Kipf, Gamaleldin F Elsayed, Aravindh Mahendran, Austin Stone, Sara Sabour, Georg Heigold, Rico Jonschkowski, Alexey Dosovitskiy, and Klaus Greff. Conditional object-centric learning from video. In *ICLR*, 2022. 3
- [20] Harold W Kuhn. The hungarian method for the assignment problem. *Naval research logistics quarterly*, 2(1-2):83–97, 1955. 7
- [21] Xiaohan Lan, Yitian Yuan, Hong Chen, Xin Wang, Zequn Jie, Lin Ma, Zhi Wang, and Wenwu Zhu. Curriculum multi-negative augmentation for debiased video grounding. In *AAAI*, 2023. 13
- [22] Jie Lei, Tamara L Berg, and Mohit Bansal. Detecting moments and highlights in videos via natural language queries. In *NeurIPS*, 2021. 2, 3, 4, 8, 9, 13, 14, 15, 16, 17, 18, 20, 21
- [23] Jie Lei, Tamara Berg, and Mohit Bansal. Revealing single frame bias for video-and-language learning. In *ACL*, 2023. 13
- [24] Jingyu Lei, Gaoang Wang, and Der-Horng Lee. CORE: Compact object-centric representations as a new paradigm for token merging in vlms. In *CVPR*, 2026. 2, 3
- [25] Juncheng Li, Junlin Xie, Long Qian, Linchao Zhu, Siliang Tang, Fei Wu, Yi Yang, Yueting Zhuang, and Xin Eric Wang. Compositional temporal grounding with structured variational cross-graph correspondence learning. In *CVPR*, 2022. 2
- [26] Junnan Li, Dongxu Li, Silvio Savarese, and Steven Hoi. Blip-2: Bootstrapping language-image pre-training with frozen image encoders and large language models. In *ICML*, 2023. 8
- [27] Yingwei Li, Yi Li, and Nuno Vasconcelos. Resound: Towards action recognition without representation bias. In *ECCV*, 2018. 13
- [28] Zeqian Li, Shangzhe Di, Zhonghua Zhai, Weilin Huang, Yanfeng Wang, and Weidi Xie. Universal video temporal grounding with generative multi-modal large language models. In *NeurIPS*, 2025. 3, 5, 8, 9
- [29] Kevin Qinghong Lin, Pengchuan Zhang, Joya Chen, Shraman Pramanick, Difei Gao, Alex Jinpeng Wang, Rui Yan, and Mike Zheng Shou. Univtg: Towards unified video-language temporal grounding. In *ICCV*, 2023. 2
- [30] Ye Liu, Kevin Qinghong Lin, Chang Wen Chen, and Mike Zheng Shou. VideoMind: A chain-of-lora agent for temporal-grounded video reasoning. In *ICLR*, 2026. 3, 8, 9
- [31] Francesco Locatello, Dirk Weissenborn, Thomas Unterthiner, Aravindh Mahendran, Georg Heigold, Jakob Uszkoreit, Alexey Dosovitskiy, and Thomas Kipf. Object-centric learning with slot attention. In *NeurIPS*, 2020. 3
- [32] Ilya Loshchilov and Frank Hutter. Decoupled weight decay regularization. In *ICLR*, 2019. 18

- [33] Boris Meinardus, Hector Rodriguez, Anil Batra, Anna Rohrbach, and Marcus Rohrbach. Chrono: A simple blueprint for representing time in mllms. In *ICCVW*, 2025. 2, 3, 5, 8, 9, 18
- [34] WonJun Moon, Sangeek Hyun, SuBeen Lee, and Jae-Pil Heo. Correlation-guided query-dependency calibration for video temporal grounding. *arXiv preprint arXiv:2311.08835*, 2023. 8, 9, 13
- [35] WonJun Moon, Sangeek Hyun, SangUk Park, Dongchan Park, and Jae-Pil Heo. Query-dependent video representation for moment retrieval and highlight detection. In *CVPR*, 2023. 2, 13
- [36] Guoshun Nan, Rui Qiao, Yao Xiao, Jun Liu, Sicong Leng, Hao Zhang, and Wei Lu. Interventional video grounding with dual contrastive learning. In *CVPR*, 2021. 13
- [37] Maxime Oquab, Timothée Darcet, Theo Moutakanni, Huy V. Vo, Marc Szafraniec, Vasil Khalidov, Pierre Fernandez, Daniel Haziza, Francisco Massa, Alaaeldin El-Nouby, Russell Howes, Po-Yao Huang, Hu Xu, Vasu Sharma, Shang-Wen Li, Wojciech Galuba, Mike Rabbat, Mido Assran, Nicolas Ballas, Gabriel Synnaeve, Ishan Misra, Herve Jegou, Julien Mairal, Patrick Labatut, Armand Joulin, and Piotr Bojanowski. DINOv2: Learning robust visual features without supervision. *arXiv:2304.07193*, 2023. 6, 7, 16, 17, 18
- [38] Mayu Otani, Yuta Nakashima, Esa Rahtu, and Janne Heikkilä. Uncovering hidden challenges in query-based video moment retrieval. *arXiv preprint arXiv:2009.00325*, 2020. 2, 13
- [39] Zhaobo Qi, Yibo Yuan, Xiaowen Ruan, ShuHui Wang, Weigang Zhang, and QingMing Huan. Bias-conflict sample synthesis and adversarial removal debias strategy for temporal sentence grounding in video. In *AAAI*, 2024. 2, 13
- [40] Shuhuai Ren, Linli Yao, Shicheng Li, Xu Sun, and Lu Hou. Timechat: A time-sensitive multimodal large language model for long video understanding. In *CVPR*, 2024. 2, 3
- [41] Maximilian Seitzer, Max Horn, Andrii Zadaianchuk, Dominik Zietlow, Tianjun Xiao, Carl-Johann Simon-Gabriel, Tong He, Zheng Zhang, Bernhard Schölkopf, Thomas Brox, et al. Bridging the gap to real-world object-centric learning. In *ICLR*, 2023. 3, 7
- [42] Hao Sun, Mingyao Zhou, Wenjing Chen, and Wei Xie. Tr-detr: Task-reciprocal transformer for joint moment retrieval and highlight detection. In *AAAI*, 2024. 2
- [43] Ye Wang, Ziheng Wang, Boshen Xu, Yang Du, Kejun Lin, Zihan Xiao, Zihao Yue, Jianzhong Ju, Liang Zhang, Dingyi Yang, Xiangnan Fang, Zewen He, Zhenbo Luo, Wenxuan Wang, Junqi Lin, Jian Luan, and Qin Jin. Time-R1: Post-training large vision language model for temporal video grounding. In *NeurIPS*, 2025. 3
- [44] Yueqian Wang, Xiaojun Meng, Jianxin Liang, Yuxuan Wang, Qun Liu, and Dongyan Zhao. HawkEye: Training video-text llms for grounding text in videos. *arXiv preprint arXiv:2403.10228*, 2024. 2, 8, 9
- [45] Ziyi Wu, Nikita Dvornik, Klaus Greff, Thomas Kipf, and Animesh Garg. Slotformer: Unsupervised visual dynamics simulation with object-centric models. In *ICLR*, 2023. 3
- [46] Jiaqi Xu, Cuiling Lan, Wenxuan Xie, Xuejin Chen, and Yan Lu. Slot-VLM: Object-event slots for video-language modeling. In *NeurIPS*, 2024. 2, 3
- [47] An Yang, Anfeng Li, Baosong Yang, Beichen Zhang, Binyuan Hui, Bo Zheng, Bowen Yu, Chang Gao, Chengen Huang, Chenxu Lv, et al. Qwen3 technical report. *arXiv preprint arXiv:2505.09388*, 2025. 7, 16, 17
- [48] Taojiannan Yang, Yi Zhu, Yusheng Xie, Aston Zhang, Chen Chen, and Mu Li. AIM: Adapting image models for efficient video understanding. In *ICLR*, 2023. 7
- [49] Xun Yang, Fuli Feng, Wei Ji, Meng Wang, and Tat-Seng Chua. Deconfounded video moment retrieval with causal intervention. In *ACM SIGIR*, 2021. 13
- [50] Yitian Yuan, Xiaohan Lan, Xin Wang, Long Chen, Zhi Wang, and Wenwu Zhu. A closer look at temporal sentence grounding in videos: Dataset and metric. In *ACM MM Workshop*, 2021. 13
- [51] Xiangyu Zeng, Kunchang Li, Chenting Wang, Xinhao Li, Tianxiang Jiang, Ziang Yan, Songze Li, Yansong Shi, Zhengrong Yue, Yi Wang, Yali Wang, Yu Qiao, and Limin Wang. TimeSuite: Improving MLLMs for long video understanding via grounded tuning. In *ICLR*, 2025. 2, 3, 8, 9
- [52] Jun Zhang, Teng Wang, Yuying Ge, Yixiao Ge, Xinhao Li, Ying Shan, and Limin Wang. Timelens: Rethinking video temporal grounding with multimodal llms. In *CVPR*, 2026. 5
- [53] Jinguo Zhu, Weiyun Wang, Zhe Chen, Zhaoyang Liu, Shenglong Ye, Lixin Gu, Yuchen Duan, Hao Tian, Weijie Su, Jie Shao, et al. InternVL3: Exploring advanced training and test-time recipes for open-source multimodal models. *arXiv preprint arXiv:2504.10479*, 2025. 3, 4, 15, 16

Appendix

In this appendix, we provide extended related work, comprehensive analyses, method details, and additional quantitative results to complement the main paper. We organize the supplementary material as follows:

- **Section A: Extended Related Work**
- **Section B: Further Analysis of the Domain Gap**
 - Section B.1: Constructing Seen/Unseen Concept Splits
 - Section B.2: Measuring Cross-Domain Visual Similarity
 - Section B.3: Analyzing the Overlap Between Concept and Visual Domain Gaps
 - Section B.4: Diagnosing on a Different MLLM
- **Section C: Further Method Details**
 - Section C.1: Extracting Subject-Object Concepts for E2V gating
 - Section C.2: Visualizing DINOv2 Cluster Maps as Supervision Signal
 - Section C.3: Implementation Details
- **Section D: Additional Experimental Results**
 - Section D.1: Analysis on the Behavior of EB Adapter
 - Section D.2: Additional Ablation Study
 - Section D.3: Qualitative Analysis of EVIDENT
- **Section E: Limitations**
- **Section F: Broader Impact**

A Extended Related Work

DETR-based VTG Specialists Prior VTG works follow the DETR paradigm [5] dominantly, where Moment-DETR [22] first cast moment retrieval as a set prediction problem and established the QVHighlights [22] benchmark. Subsequent models extend this paradigm by injecting VTG-specific inductive biases into the decoder, such as query-dependent representations [35], event-aware attention [16], and correlation-guided calibration [34].

Bias in Video Understanding Dataset bias has been extensively investigated across various video understanding tasks. In action recognition, Choi et al. [9] show that models often rely on scene context as a shortcut, achieving high accuracy without truly recognizing the action itself. Li et al. [27] formalize the notion of representation bias in video datasets and propose the Diving48 benchmark to address it. Bae et al. [2] further tackle this issue by learning disentangled representations of action and scene. Beyond action recognition, Lei et al. [23] report that single-frame models achieve surprisingly competitive results on video-language tasks, highlighting a static appearance bias.

Within the VTG domain, Otani et al. [38] show that blind baselines without any video input can rival trained models by leveraging annotation distribution patterns. This observation motivated the construction of out-of-distribution evaluation splits [50] and a line of debiasing methods. Causal inference approaches [49, 36] apply backdoor adjustment to mitigate the confounding effect of moment location. Adversarial and augmentation-based strategies [39, 12, 21] either generate bias-conflict samples or perturb the temporal structure to discourage shortcut learning. Chae et al. [6] introduce a comprehensive benchmark over seven datasets and analyze annotation bias and query text patterns. Together, these studies indicate that VTG datasets exhibit a wide range of biases across annotation distributions, language patterns, and visual modalities, and that existing models remain susceptible to such shortcuts instead of performing genuine cross-modal grounding.

B Further Analysis of the Domain Gap

B.1 Constructing Seen/Unseen Concept Splits

For the concept domain gap analysis shown in Figure 3 (a), we partition the QVHighlights (QVH) [22] test set into *seen* and *unseen* concept subsets with respect to the Charades-STA (Cha.) [10] training

distribution. Specifically, we first build a Cha.-centric concept vocabulary \mathcal{C} by taking the 50 most frequent content lemmas across all Cha. training queries, after standard lowercasing, lemmatization, and stop-word removal. The resulting set covers the dominant indoor activity, object, and motion vocabulary of Cha. (e.g. *glass, walk, sneeze, room, door, cup, shelf, sit, pillow, refrigerator, blanket*). Each QVH test query is then processed with the identical pipeline, and labeled *seen* if at least one of its lemmas appears in \mathcal{C} , otherwise *unseen*. This rule yields 635/915 seen/unseen samples out of 1,550; to remove the class-size imbalance, we draw a fixed random subset of 600 samples from each group as our final evaluation splits. We use only word-level lemma matching, without expanding to a hand-crafted concept ontology, so that the split reflects lexical familiarity to the Cha.-trained model without additional human bias.

B.2 Measuring Cross-Domain Visual Similarity

For the visual domain gap analysis shown in Figure 3 (b), we embed each video as a single global descriptor by passing 20 uniformly sampled 224×224 frames through a frozen Qwen2.5-VL-3B [3] vision encoder, mean-pooling visual tokens within each frame and then averaging the resulting per-frame vectors. Taking Charades-STA (Cha.) [10] training videos as the reference distribution, we define a centroid $\mathbf{c}_{\text{Cha.}}$ as the mean of their global descriptors, and characterize each test video by its cosine similarity $s(v) = \cos(\mathbf{v}, \mathbf{c}_{\text{Cha.}})$ to this centroid. While the Cha. training set is internally tight (intra-set similarity 0.894 ± 0.035 over 5,335 videos), QVHighlights (QVH) [22] test videos drift toward lower similarities (0.831 ± 0.061 , range $[0.527, 0.942]$ over 1,519 videos), indicating a measurable train→test visual shift (Figure 6).

We sort the QVH test set by $s(v)$ and partition it into five equally sized quantile bins (Figure 6). Reporting performance on the top and bottom quantiles—denoted **Visually similar** (Q1, $s \geq 0.881$) and **Visually dissimilar** (Q5, $s \leq 0.789$)—isolates the impact of the visual domain gap on temporal grounding without conflating it with other dataset-specific factors. Note that the cosine values themselves are meaningful only as relative scores within the Qwen2.5-VL [3] embedding space; we use them solely to induce an ordering over test videos.

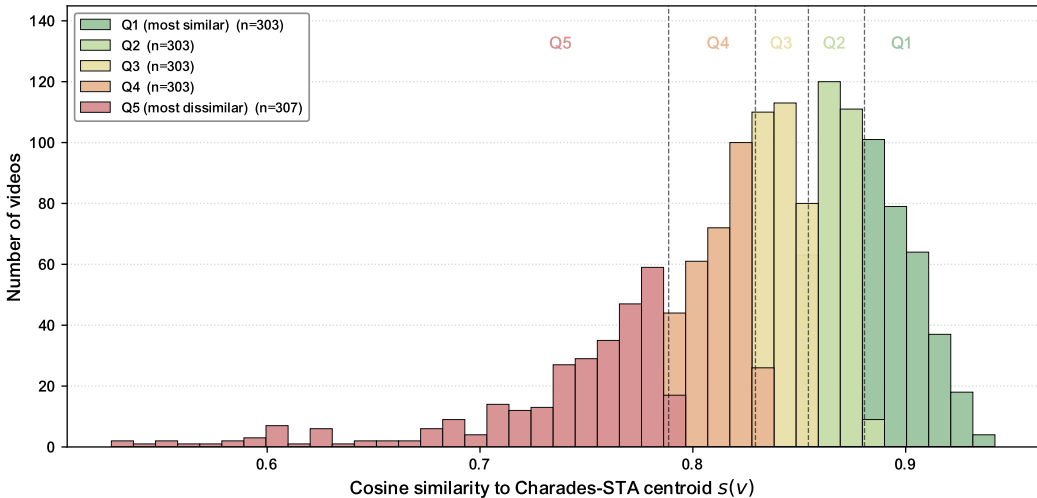


Figure 6: **Visual similarity distribution and quintile partitioning.** Distribution of cosine similarities $s(v) = \cos(\mathbf{v}, \mathbf{c}_{\text{Cha.}})$ between QVHighlights [22] test video descriptors \mathbf{v} and the Charades-STA [10] training centroid $\mathbf{c}_{\text{Cha.}}$, computed in a frozen Qwen2.5-VL-3B [3] embedding space. The 1,519 test videos (1,550 query samples) are sorted by $s(v)$ and partitioned into five equally sized quantile bins (dashed lines). We evaluate temporal grounding on the highest- and lowest-similarity bins, **Q1** (*Visually similar*, $s \geq 0.881$) and **Q5** (*Visually dissimilar*, $s \leq 0.789$), to isolate the effect of visual domain shift. Cosine values are relative scores within this encoder’s embedding space and are not directly comparable to similarities computed under a different encoder.

B.3 Analyzing the Overlap Between Concept and Visual Domain Gaps

A natural concern is whether our two evaluation axes used in Figure 3—the concept-based split (a) and the visual-similarity split (b)—reflect the same underlying train-test gap. To examine this, we cross-tabulate the 1,200 QVHighlights (QVH) [22] samples that appear in both splits and report the joint distribution in Table 3.

Table 3: **Joint distribution of QVHighlights samples across concept and visual splits.** How the 1,200 QVHighlights [22] test samples split across the two axes. Rows group samples by query concept (Seen vs. Unseen Charades-STA [10]-style vocabulary); columns group videos by visual similarity to Charades-STA, from Q1 (closest) to Q5 (farthest).

	Q1 (closest)	Q2	Q3	Q4	Q5 (farthest)	Total
Seen	145	127	123	103	102	600
Unseen	103	121	112	130	134	600
Total	248	248	235	233	236	1,200

If the two splits captured the same factor underlying the OOD gap, Seen samples would pile up in the visually closest bins (Q1–Q2) and Unseen samples in the farthest (Q4–Q5), giving a clear diagonal pattern. What we actually see is only a mild lean in that direction: the Seen group is slightly more common in Q1 (145 vs. 103) and slightly less common in Q5 (102 vs. 134), but every bin contains a substantial proportion of both groups. Even Q1—the videos most similar to Charades-STA [10]—shows a 58:42 split between Seen and Unseen, far from the near-100:0 distribution we would expect under full overlap.

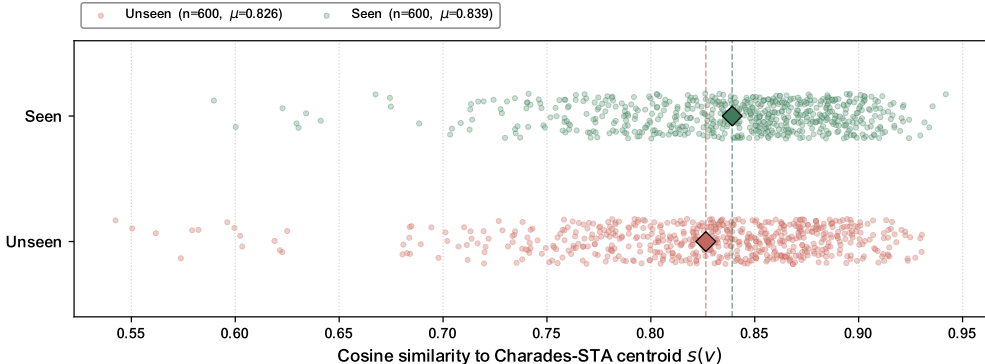


Figure 7: **Concept and visual axes carry independent information.** Each dot is one of the 1,200 QVHighlights [22] test samples, plotted at its cosine similarity $s(v)$ to the Charades-STA [10] centroid (x-axis); samples are split into two lanes by query concept (Seen / Unseen). Diamonds mark the per-group mean. The two lanes occupy nearly the same range of $s(v)$ and their means sit only 0.013 apart, suggesting that the concept and visual axes carry independent information.

Pearson correlation on the continuous similarity score. For a complementary view that uses the raw similarity score rather than quintile bins, Figure 7 plots each sample at its $s(v)$. The Pearson correlation between the binary concept indicator (Seen = 1, Unseen = 0) and $s(v)$ over $N=1,200$ samples is $\rho = +0.106$ ($p = 2.3 \times 10^{-4}$): Seen samples sit at a slightly higher mean similarity (0.839 vs. 0.826), but the concept group explains only $R^2 \approx 1.1\%$ of the variance in $s(v)$. The two axes are therefore *statistically* but not *practically* associated.

B.4 Diagnosing on a Different MLLM

To verify that our problem analysis is not specific to Qwen2.5-VL [3], we replicate the analyses of Figure 2 and Figure 3 on a different MLLM, InternVL3-2B [53]. As shown in Figure 8, InternVL3-2B exhibits the same pattern as Qwen2.5-VL reported in Section 3.

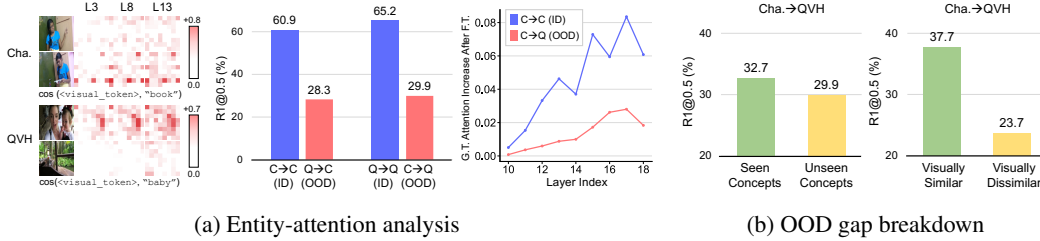


Figure 8: **Problem analysis on InternVL3-2B [53]**. We replicate the analysis of Figure 2 and Figure 3 on a different MLLM, InternVL3-2B, and observe the same pattern as Qwen2.5-VL [3] reported in Section 3. **(a) Entity-attention analysis.** (Left) Zero-shot entity-attention exhibits strong visual-text alignment regardless of the video domain. (Middle) Naïve fine-tuning suffers severe ID-OOD gaps. (Right) After fine-tuning, the attention on ground-truth-interval frames substantially increases on the trained domain (ID) but only marginally on the unseen domain (OOD), indicating that the learned visual-text alignment ability fails to transfer to other domains. **(b) OOD gap breakdown.** (Left) Splitting the OOD test set by query-concept overlap with ID yields only a marginal performance gap, indicating that the concept gap is not the dominant factor. (Right) Splitting OOD samples by visual feature similarity to ID yields a much larger gap, identifying the visual domain gap as the primary cause of OOD degradation.

Entity-attention analysis (Figure 8 (a)). The zero-shot InternVL3-2B exhibits strong visual-text alignment across both Charades-STA [10] and QVHighlights [22], but naïve fine-tuning suffers severe ID-OOD performance gaps. The fine-tuned model’s attention on ground-truth-interval frames substantially increases on the trained domain (ID) but only marginally on the unseen domain (OOD), indicating that the learned visual-text alignment ability fails to transfer to other domains.

OOD gap breakdown (Figure 8 (b)). Splitting the OOD test set by query-concept overlap with ID yields only a marginal performance gap, while splitting by visual feature similarity to ID yields a much larger gap. This identifies the visual domain gap as the primary cause of OOD degradation, consistent with our observations on Qwen2.5-VL. Together, these results suggest that entity-attention bypass under visual domain shift is a general phenomenon across MLLMs rather than a model-specific artifact.

C Further Method Details

C.1 Extracting Subject-Object Concepts

Entity-to-evidence (E2V gating, Section 4.4) takes a subject-object concept pair as textual input. For each training query, we extract this pair by prompting Qwen3-4B-Instruct-2507 [47] in a zero-shot (Figure 9) to return a JSON object with two entries: a `Subject`: (primary actor) and an `Object`: (tangible interaction target), each restricted to a 1–2 word noun. Given the extracted concept words, we identify their token positions in the original query token sequence as i_{sub} and i_{obj} , which are then used to select the corresponding query token features \mathbf{q}'_{sub} and \mathbf{q}'_{obj} for E2V gating. This schema deliberately excludes verbs, scenes, and abstract descriptions so that the resulting concepts correspond to *visually grounded* entities that align with frame-level evidence during E2V gating.

C.2 Visualizing DINOv2 Cluster Maps as Supervision Signal

Our EB Distillation relies on DINOv2 [37] K -means cluster maps as pseudo-ground-truth supervision for slot attention. To verify the reliability of this supervision signal, we examine whether DINOv2 features produce semantically meaningful clusters.

We visualize DINOv2 cluster maps on videos from our evaluation benchmarks. Concretely, we extract DINOv2-large patch features for 20 uniformly sampled 224×224 frames, apply 2×2 average pooling to reduce each frame to a 8×8 spatial grid (64 patches), ℓ_2 -normalize the features, and run K -means with $K=4$. Figure 10 shows the resulting cluster assignments: for each cluster, we display only the patches assigned to that cluster.

User

You are an expert in semantic decomposition for video temporal grounding. Extract the most important Subject and Object from the query for frame-level grounding.

Roles & Prefixes you MUST use:

- "Subject : [noun] " → The primary living actor or main entity.
- "Object : [physical noun] " → The primary tangible target object being interacted with. If none exists, omit this.

Rules:

1. Return a JSON list containing up to 2 strings.
2. Each string MUST start with "Subject : " or "Object : ".
3. If the Subject is interacting with a physical item, you MUST extract it as an Object.
4. Ignore verbs, scenes, abstract concepts, and meta-descriptions.
5. Keep the nouns extremely concise (1–2 words).
6. Return ONLY a valid JSON list.

Examples:

Query: “a person opens the refrigerator in the kitchen”
 JSON list: ["Subject: person", "Object: refrigerator"]

Query: “The girl dances around the room.”
 JSON list: ["Subject: girl"]

Query: {query}
 JSON list:

Assistant

JSON list of extracted concepts

Figure 9: Zero-shot prompt used with Qwen3-4B-Instruct-2507 [47] for key concept extraction. Blue text represents variables.

The results demonstrate that DINOv2 *K*-means clusters naturally partition frames into semantically coherent regions—consistently separating foreground actors, interaction targets, background scene elements, and motion-salient regions. This confirms that using DINOv2 cluster maps as pseudo-GT for EB Distillation provides a semantically grounded training signal rather than an arbitrary one, justifying our design choice. As shown in the bottom row of Figure 10, slots trained with our EB Distillation mirror this DINO structure, binding each slot to a distinct entity consistently across both ID and OOD domains.

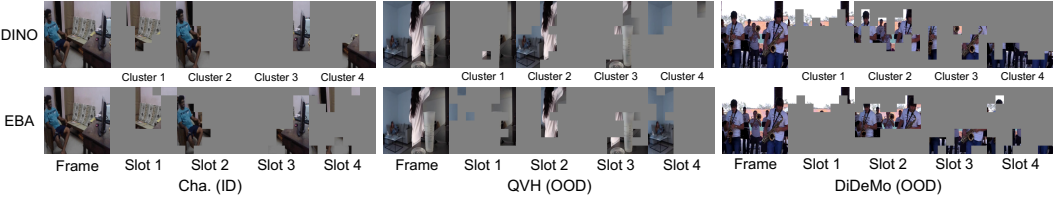


Figure 10: **DINOv2 cluster maps vs. EB Adapter slot assignments.** Each group shows a frame and four isolated patch views across Charades-STA (Cha.) [10] (ID), QVHighlights (QVH) [22](OOD), and DiDeMo [13] (OOD). **Top (DINO):** DINOv2 [37] *K*-means naturally separates semantically coherent regions, validating its use as pseudo-ground-truth in EB Distillation. **Bottom (EB Adapter):** Slots trained with EB Distillation mirror the DINO structure, binding each slot to a distinct entity consistently across domains.

Table 4: **Fine-tuning setting of EVIDENT.**

Category	Hyperparameter	Charades-STA [10]	QVHighlights [22]
Input	# Frames	20	60
	Resolution	224 × 224	
Optimization	Optimizer	AdamW [32]	
	Learning rate	5×10^{-5}	
	LR scheduler	Cosine, 5% warmup	
	Weight decay	0.1	
	Epochs	2	
	Global batch size	32	
LoRA	Applied layers	11–27	
	Rank r	16	
	α	64	
	Dropout	0.05	
EB Adapter	Inserted layers	0–10	
	# Slots K	4	
	Bottleneck dim	896	
	# Iterations	3	
	Tokens per frame	64	
EB Distillation	Loss weight λ	0.1	1.0

C.3 Implementation Details

We build upon Qwen2.5-VL-Instruct [3] (7B) as the backbone MLLM, where the LLM decoder has a hidden dimension of $D=3584$. The vision encoder processes each 224×224 frame into $N=64$ visual tokens (8×8 spatial grid). For the EB Adapter, we set the bottleneck dimension to $d=896$, the number of slots to $K=4$, and use 8 attention heads with $I=3$ iterations of GRU-based refinement. We inject the EB Adapter into layers 0–10, while LoRA [14] (rank 16, $\alpha=64$) is applied to the remaining deeper layers; the vision tower, the LLM’s frozen layers, and the vision–language merger are kept fixed throughout training. The E2V gating module is applied at every EB Adapter layer (0–10) and modulates the slot residual using the cosine similarity between subject/object queries and per-frame mean-pooled visual tokens. The EB Distillation derives pseudo-GT cluster maps by K -means clustering DINOv2-large [37] patch features, and aligns slot-attention maps to these clusters via Hungarian matching with BCE loss at every EB Adapter layer (0–10) with $\lambda=0.1$.

Video sampling and timestamps. We uniformly sample 20 and 60 frames for the models trained on Charades-STA [10] and QVHighlights [22], respectively. For cross-domain evaluation, we follow each *target* dataset’s native protocol and sample 20 frames for Charades-STA, 60 frames for QVHighlights, and 20 frames for DiDeMo [13]. For Charades-STA training, whose clips are confined to a narrow 0–30s range, we further adopt the *relative-integer* timestamp encoding of Chrono-BLIP [33], representing each timestamp as an integer in $[0, 100]$ relative to clip duration; this mitigates the text bias toward a narrow band of numeric tokens that the dataset’s limited duration range would otherwise induce.

Gating under partial concept queries. Not every query specifies both a subject and an object: queries such as “*a person is dancing*” contain a subject but no object. For such samples, we pass the absent concept’s score through as 1 rather than 0: since the per-frame gate is the multiplicative product of the two scores, 1 is its identity element, so the absent concept exerts no influence on gating while the present one continues to drive it—whereas 0 would collapse the gate regardless of the present concept’s signal.

Optimization. We train for 2 epochs with AdamW [32] (learning rate 5×10^{-5} , weight decay 0.1) under a cosine schedule with 5% linear warmup, using a global batch size of 32 on 8 NVIDIA 3090/4090 GPUs. Full hyperparameter details are summarized in Table 4. In total, the trainable parameters amount to approximately 201M (2.36% of the backbone) for the 7B model.

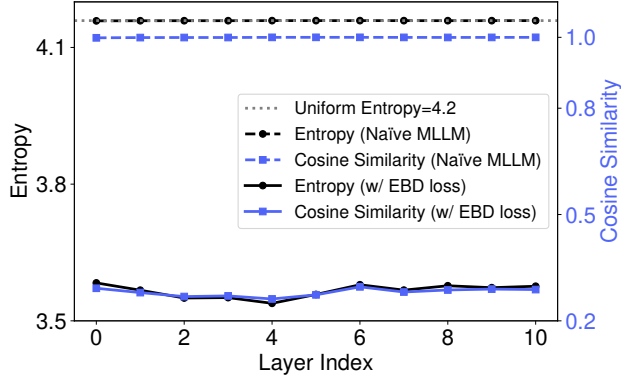


Figure 11: **Analysis on slot attention weights in EB Adapter.** We plot the entropy and pairwise cosine similarity of normalized slot attention weights in EB Adapter across layers. The naïve MLLM visual space yields nearly *uniform* attention, indicating no entity-level binding, whereas our EB Distillation loss yields lower entropy and cosine similarity—evidence that each slot captures a distinct entity.

D Additional Experimental Results

D.1 Analysis on the Behavior of EB Adapter

We further analyze the internal behavior of EB Adapter by examining its slot attention weights $\hat{\mathbf{A}}$. Specifically, we measure two complementary properties across all EB Adapter layers (Figure 11): (i) the *entropy* of each slot’s attention distribution over visual tokens, which quantifies how concentrated each slot is on specific regions, and (ii) the *pairwise cosine similarity* between slots, which quantifies whether different slots attend to distinct regions.

Without our EB Distillation loss, the naïve MLLM visual space yields nearly *uniform* attention weights (entropy approaching the theoretical uniform bound of 4.2) and near-perfect inter-slot cosine similarity (≈ 1.0), indicating that all slots collapse to attending to the same diffuse region rather than binding to distinct entities. This confirms that the intermediate visual representation of a pre-trained MLLM does not afford entity-level binding on its own.

In contrast, training EB Adapter with our EB Distillation loss drives both metrics down substantially: the entropy drops to around 3.5 and the inter-slot cosine similarity drops to around 0.3 across all layers. This indicates that each slot attends to a sharper, more localized region and that different slots attend to disjoint regions, providing direct evidence that EB Distillation successfully encourages each slot to bind to a distinct entity.

D.2 Additional Ablation Study

We provide further ablations on the design choices of EB Distillation and E2V gating in Table 5.

(a) Effects of EB Adapter insertion layers. We show that inserting the EB Adapter into decoder layers 0–10 yields the best OOD performance. As discussed in Section 4.2, this choice places our EB Adapter in the early layers where cross-frame interactions occur [18], allowing each slot to capture temporally coherent disentangled semantics. Meanwhile, the mid-to-later layers responsible for vision-language integration [18] are left to lightweight LoRA [14] fine-tuning, preventing excessive overfitting to the source domain.

(b) Effects of token reconstruction design. We demonstrate that reusing the slot attention weights to reconstruct the original token sequence, mentioned in Section 4.2, substantially improves OOD performance (+2.1 points in R1@0.5). This attention reuse design routes VTG adaptation through disentangled entity-level representations and eliminates the additional learnable parameters that could overfit to the source domain.

(c) Effects of EB Distillation loss scale and placement. We ablate the loss weight λ and the layer indices at which EB Distillation is applied. Across the three loss scales tested under the all-layer setting (0–10), the differences are minor: ID and OOD metrics remain within roughly 1–2 points

across $\lambda \in \{1.0, 0.5, 0.1\}$, indicating that EB Distillation is robust to the choice of loss scale. Our default $\lambda=0.1$ achieves the best ID R1@0.5 (69.1) and OOD R1@0.7 (36.9), while $\lambda=1.0$ slightly favors OOD R1@0.5 (60.4 vs. 59.8). Restricting EB Distillation to only the last EB Adapter layer ($l=10$) leads to a small but consistent drop across metrics, suggesting that progressively applying EB Distillation across all EB Adapter layers (0–10) is mildly more effective than aligning only the final layer.

(d) Effects of visual feature source in E2V gating. We ablate which visual feature is used to compute the per-frame gating score, comparing tokens *before* down projection, *after* down projection, and *after* slot-based reconstruction. Features *after* down projection give the best overall performance, achieving the highest OOD scores (R1@0.5 of 59.8) while remaining competitive on ID. Pre-projection features underperform on both splits, and post-reconstruction features collapse on OOD (R1@0.5 drops to 51.9), as the slot bottleneck discards fine-grained details needed for entity-level scoring. This indicates that E2V gating should be computed from the LLM’s visual stream rather than the bottlenecked slot output.

(e) Effects of E2V gating applied layers. We ablate whether E2V gating should be applied at every EB Adapter layer (L0–10) or only at the final layer (L10). Applying E2V gating across all EB Adapter layers consistently outperforms the last-layer-only variant on OOD R1@0.5 (59.8 vs. 55.8) while maintaining competitive ID performance. This shows that progressively gating the slot residual at every layer better aligns the entity-level representations with query-relevant frames, leading to more robust cross-domain generalization.

Table 5: **Additional Ablation Study.** Further ablations on the formulation of EB Distillation and the detailed configurations of E2V gating.

(a) Effects of EB Adapter insertion layers.					(b) Effects of token reconstruction design.				
Layer Index i	Cha. (ID)		QVH (OOD)		Method	Cha. (ID)		QVH (OOD)	
	R1@0.5	R1@0.7	R1@0.5	R1@0.7		R1@0.5	R1@0.7	R1@0.5	R1@0.7
0-6	69.2	49.5	56.8	34.9	Cross attention	69.0	49.3	57.7	35.1
0-10	69.1	49.2	59.8	36.9	Attention reuse	69.1	49.2	59.8	36.9
0-14	69.1	49.4	58.3	33.7					

(c) Effects of EB Distillation loss and placement.					(d) Effects of visual feature source in E2V gating.					
Loss scale λ	Layer index l	Cha. (ID)		QVH (OOD)		Visual feature	Cha. (ID)		QVH (OOD)	
		R1@0.5	R1@0.7	R1@0.5	R1@0.7		R1@0.5	R1@0.7	R1@0.5	R1@0.7
1.0	0-10	68.3	49.2	60.4	36.0	Before down proj.	68.4	49.0	55.8	34.1
0.5	0-10	68.7	49.3	58.4	34.9	After down proj.	69.1	49.2	59.8	36.9
0.1	0-10	69.1	49.2	59.8	36.9	After token reconstruction	69.2	50.3	51.9	29.7
0.1	10	68.7	49.0	57.9	36.5					

(e) Effects of E2V gating applied layers.				
E2V gating Layers	Cha. (ID)		QVH (OOD)	
	R1@0.5	R1@0.7	R1@0.5	R1@0.7
Only last layer (L10)	68.9	49.8	55.8	36.2
All adapter layers (L0-10)	69.1	49.2	59.8	36.9

D.3 Qualitative Analysis of EVIDENT

Slot visualization in temporal order As shown in Figure 12, each slot consistently attends to the same entity across consecutive frames, forming temporally coherent trajectories along the time axis. Regions corresponding to the same slot (i.e., the same color) remain stable as the scene evolves, indicating that EB Adapter binds each slot to a specific entity and tracks it over time rather than re-assigning slots arbitrarily at each frame. This temporal continuity is observed not only on the in-domain Charades-STA [10] samples but also on out-of-domain QVHighlights [22] and DiDeMo [13] samples, suggesting that the learned slot-entity binding generalizes beyond the training distribution.

Gating score visualization In Figure 13, we visualize the gating scores of each entity produced by E2V gating on Charades-STA [10] (ID) and QVHighlights [22] (OOD) samples. We observe that the gating scores computed by EVIDENT accurately reflect the temporal intervals in which each entity appears in the visual content.

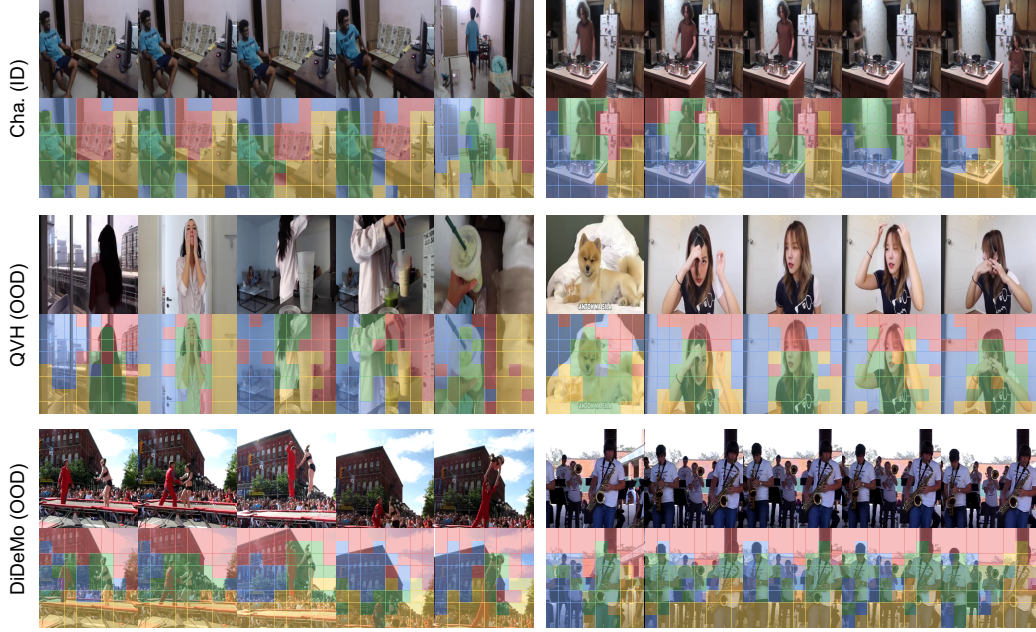


Figure 12: **EB Adapter visualization.** We visualize the slot assignments on samples from Charades-STA (Cha.) [10] (ID), QVHighlights (QVH) [22] (OOD), and DiDeMo [13] (OOD) by masking each frame with its highest-attending slot. Frames are arranged in temporal order from left to right, and the same color denotes the same slot.

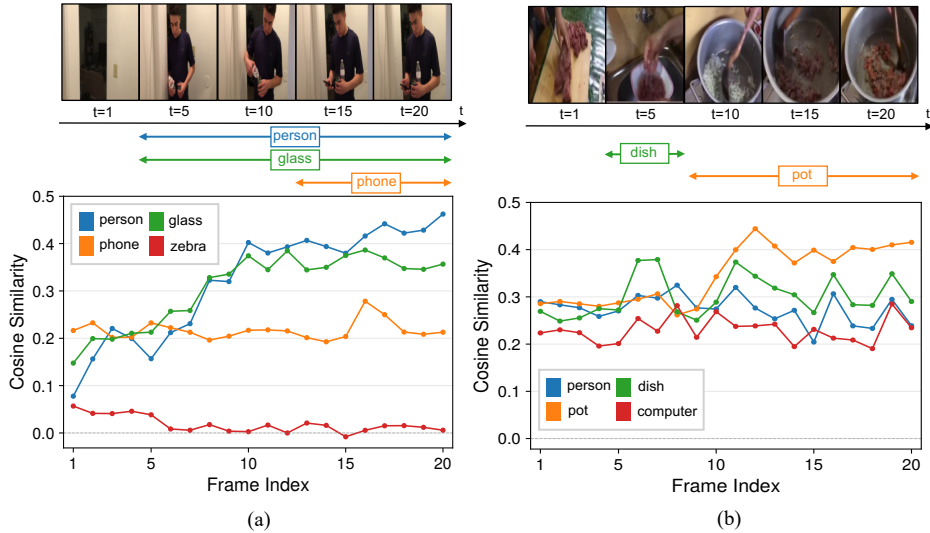


Figure 13: **E2V gating score visualization.** We visualize the per-entity gating scores from E2V gating (see Section 4.4) on (a) Charades-STA [10] (ID) and (b) QVHighlights [22] (OOD) samples.

E Limitations and Future Work

EVIDENT addresses cross-domain VTG under visual distribution shift, with experiments spanning three diverse benchmarks (Charades-STA, QVHighlights, DiDeMo). Extending our analysis to more challenging settings such as long-form videos, egocentric perspectives, or open-vocabulary temporal grounding is a promising direction for future work. While we identify visual domain shift as the dominant failure mode of naïvely fine-tuned MLLMs, jointly addressing other forms of distribution shift, such as temporal granularity or query style, would require complementary advances. We

view EVIDENT as a first step toward systematically diagnosing and mitigating distribution shifts in MLLM-based video temporal grounding.

F Broader Impact

EVIDENT improves the robustness of MLLM-based video temporal grounding under domain shift, with potential positive impacts on applications such as video search, content accessibility (e.g., caption alignment for visually impaired users), and video understanding tools for education and media analysis. By promoting entity-grounded reasoning rather than reliance on dataset-specific shortcuts, our framework may also reduce systematic biases inherited from training data, contributing to more reliable model behavior in unseen scenarios. We do not foresee direct negative societal impacts from this work, as it builds on publicly available pre-trained models and datasets and does not enable new generative or surveillance capabilities. Standard considerations applicable to general video understanding research—such as privacy concerns when applying such systems to personal video content—should be observed by downstream users.